

MAPPING CRUSTAL HEATING WITH THE COOLING LIGHTCURVES OF QUASI-PERSISTENT TRANSIENTS

EDWARD F. BROWN

Department of Physics & Astronomy, National Superconducting Cyclotron Laboratory, and the Joint Institute for Nuclear Astrophysics, Michigan State University, East Lansing, MI 48824

AND

ANDREW CUMMING

Department of Physics, McGill University, 3600 rue University, Montreal, QC, H3A2T8, Canada
to appear in The Astrophysical Journal

ABSTRACT

The monitoring of quiescent emission from neutron star transients with accretion outbursts long enough to significantly heat the neutron star crust has opened a new vista onto the physics of dense matter. In this paper we construct models of the thermal relaxation of the neutron star crust following the end of a protracted accretion outburst. We confirm the finding of Shternin et al., that the thermal conductivity of the neutron star crust is high, consistent with a low impurity parameter. We describe the basic physics that sets the broken power-law form of the cooling lightcurve. The initial power law decay gives a direct measure of the temperature profile, and hence the thermal flux during outburst, in the outer crust. The time of the break, at hundreds of days post-outburst, corresponds to the thermal time where the solid transitions from a classical to quantum crystal, close to neutron drip. We calculate in detail the constraints on the crust parameters of both KS 1731–260 and MXB 1659–29 from fitting their cooling lightcurves. Our fits to the lightcurves require that the neutrons do not contribute significantly to the heat capacity in the inner crust, and provide evidence in favor of the existence of a neutron superfluid throughout the inner crust. Our fits to both sources indicate an impurity parameter of order unity in the inner crust.

Subject headings: dense matter — stars: neutron — X-rays: binaries — X-rays: individual(KS 1731–260, MXB 1659–29)

1. INTRODUCTION

In 2001 the low mass X-ray binary KS 1731–260 went into quiescence (Wijnands et al. 2001) after accreting steadily since its first detection about 12 years prior (Sunyaev 1989). Rutledge et al. (2002) suggested that the neutron star crust would be heated out of thermal equilibrium with the core during this long outburst, and that monitoring observations could detect the thermal relaxation of the crust following the cessation of accretion. A regular monitoring program of KS 1731–260 with Chandra and XMM (Wijnands et al. 2001; Wijnands et al. 2002; Cackett et al. 2006) has indeed detected a steadily decaying luminosity. Another source, MXB 1659–29, has also been observed to cool following a 2.5 yr-long outburst (Wijnands et al. 2003; Wijnands et al. 2004), and recent observations show that the cooling appears to have halted (Cackett et al. 2008). Recently a third source, AX J1754.2–2754, was observed to turn off (Bassa et al. 2008) after being in outburst since being detected in 1999 (Sakano et al. 2002). This source is likely an ultracompact binary, and is of particular interest as it may be similar to 1H 1905+000, which has an extremely low quiescent flux, perhaps indicating a very low neutron star core temperature (Jonker et al. 2006). Finally, the rapidly accreting source XTE J1701–462 went into quiescence in 2007 after ≈ 1.6 yr of active accretion (Homan et al. 2007; Altamirano et al. 2007), and EXO 0748–676 entered quiescence in 2008 after being in outburst for 24 yr (Degenaar et al. 2009).

Rutledge et al. (2002) emphasized that observations of the crust cooling would offer a new probe of the crust thermal properties. The crust of a neutron star in a LMXB may have

significantly different properties than that of a young isolated neutron star, as the accretion lifetime of a LMXB is long enough for accreted matter to replace the entire crust. The accreted crust is heated during outburst by electron captures and pycnonuclear reactions, mostly at densities close to neutron drip (Haensel & Zdunik 1990, 2003, 2008). The temperature profile in the crust is determined by how the heat released in this “deep crustal heating” is transported outwards to the surface or inwards to the neutron star core, where it is radiated as neutrinos.

A particularly uncertain property of accreted crusts is the thermal conductivity. The matter entering the top of the crust is expected to consist of a mixture of elements produced by hydrogen and helium burning at low densities. Schatz et al. (1999) found that rp-process burning produced ashes with $Q_{\text{imp}} \approx 100$, where the impurity parameter

$$Q_{\text{imp}} \equiv n_{\text{ion}}^{-1} \sum_i n_i (Z_i - \langle Z \rangle)^2 \quad (1)$$

measures the distribution of nuclide charge numbers, an important parameter for setting the conductivity of the crust (Itoh & Kohyama 1993). Brown (2000) suggested that at such large values of Q_{imp} , the crust would have an amorphous structure, with a low thermal conductivity comparable to the conductivity of the liquid state. Recent molecular dynamics calculations of the solidification of such a mixture (Horowitz et al. 2007, 2008a) show, however, that a regular crystal structure does form, but that phase separation between the liquid and solid phases or the formation of multiple solid phases can occur, changing the effective value of Q_{imp} in the crust compared to the rp-process mixture. In addition, nuclear reactions in the crust may also act to reduce the effective value of Q_{imp}

(Horowitz et al. 2008a). Measurement of Q_{imp} in the crust would therefore give an important test of the composition of rp-process ashes and their subsequent evolution as they are compressed towards nuclear density.

Shternin et al. (2007) compared time-dependent calculations of deep crustal heating and subsequent cooling to the observations of KS 1731–260. They found that a low value of thermal conductivity corresponding to an amorphous crust could be ruled out because it would give cooling on a much longer timescale than observed. In this paper, we confirm this result, and go further by describing the basic physics that sets the shape of the cooling lightcurve, and calculating in detail the constraints on Q_{imp} and other crust parameters coming from the cooling lightcurves of both KS 1731–260 and MXB 1659–29. Cackett et al. (2006) found that both of these decays could be fit with an exponential decay to a constant, although a single power-law ($L \propto t^{-\alpha}$, with $\alpha = 0.50 \pm 0.03$) also adequately fits the data for KS 1731–260 (Cackett et al. 2008). We show here that the lightcurve of a cooling crust is a broken power law. The initial power law decay gives a direct measure of the temperature profile, and hence the thermal flux during outburst, in the outer crust. The time of the break, at hundreds of days post-outburst, corresponds to the thermal time where the solid transitions from a classical to quantum crystal, close to neutron drip. At late times, the luminosity levels off at a value set by the neutron star core temperature.

We start in §2 by describing our time-dependent cooling calculations and an analytic model of the results, and go on in §3 to calculate the constraints on crust parameters coming from comparison with the observed cooling of KS 1731–260 and MXB 1659–29. The Appendix discusses the details of our crust models.

2. MODELS OF CRUST COOLING IN KS 1731–260 AND MXB 1659–29

2.1. Hydrostatic structure of the crust

Because the temperature is always low relative to the electron and neutron Fermi energies, we can solve for the temperature and luminosity using a hydrostatic structure. In the crust, the pressure P makes a convenient Eulerian coordinate, and we integrate the equations (Thorne 1977) for the radius r , gravitational mass M , and potential ϕ ,

$$\frac{dr}{d \ln P} = -\frac{P}{\rho g} (1+z)^{-1}, \quad (2)$$

$$\frac{dM}{d \ln P} = -4\pi r^2 \frac{P}{g}, \quad (3)$$

$$\frac{d\phi}{d \ln P} = -\frac{P}{\rho}. \quad (4)$$

Here $1+z = [1 - 2GM/(rc^2)]^{-1/2}$, $g = GM(1+z)/r^2$ is the gravitational acceleration, and ρ is the density of mass-energy. We have neglected terms $O(\rho r^3/Mc^2)$, as appropriate in the crust. As boundary conditions, we assume a transition density to uniform npe matter at $n = 0.08 \text{ fm}^{-3}$ (consistent with recent studies of clustering in uniform nuclear matter; Oyatsu & Iida 2007), and set M and r according to a neutron star model computed using the EOS of Akmal et al. (1998). We integrate outwards to a pressure $P = 2.3 \times 10^{26} \text{ ergs cm}^{-3}$, corresponding to a column depth from the surface¹ of $P/g =$

¹ In a thin layer, the column depth is $\int_r^\infty \rho dr \approx P/g$; in this paper we will use the term to refer to $y \equiv P/g$.

$10^{12} \text{ g cm}^{-2}$, at which point we apply the third boundary condition $\phi(r=R) = (c^2/2) \ln[1 - 2GM/(Rc^2)]$. The integration is performed using a standard fourth-order Runge-Kutta algorithm, and the output is constrained to generate points uniformly distributed in $\ln P$ for use in the time-dependent code (§ 2.2). Our equation of state, as well as our model for the composition, is detailed in the Appendix.

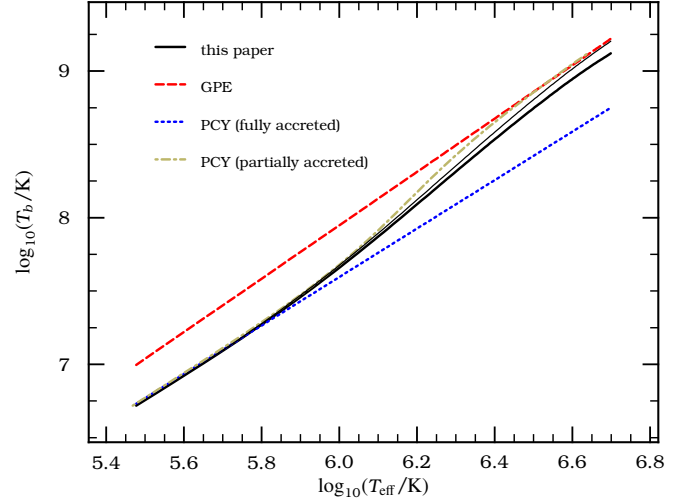


FIG. 1.— Temperature in the neutron star ocean (T_b) as a function of photosphere temperature T_{eff} (solid line). The relation of Gudmundsson et al. (1983, dashed line) is shown for comparison. We also show two models from Potekhin et al. (1997): their “fully accreted” model dotted line and a “partially accreted” model dot-dashed line in which the light elements are in the region $P/g < 10^9 \text{ g cm}^{-2}$. Note that for these latter two models, the temperature T_b is taken at a density $10^{10} \text{ g cm}^{-3}$ ($P/g \approx 4.3 \times 10^{13} \text{ g cm}^{-2}$), which is somewhat deeper than the boundary used in our calculations. For comparison with these cases, we also show (thin solid line) our relation obtained by integrating to this depth.

2.2. Time-dependent Heating and Cooling

The time-dependent equations for the evolution of temperature and luminosity are

$$\frac{\partial}{\partial t} (T e^{\phi/c^2}) = e^{2\phi/c^2} \frac{\epsilon_{\text{nuc}} - \epsilon_\nu}{C} - \frac{1}{4\pi r^2 \rho C (1+z)} \frac{\partial}{\partial r} (L e^{2\phi/c^2}) \quad (5)$$

$$L e^{2\phi/c^2} = -\frac{4\pi r^2 K e^{\phi/c^2}}{1+z} \frac{\partial}{\partial r} (T e^{\phi/c^2}), \quad (6)$$

where ϵ_{nuc} and ϵ_ν are the specific nuclear heating and neutrino emissivity, C is the specific heat, and K is the thermal conductivity. We solve these equations using the method of lines. We use the common technique of defining $L e^{2\phi/c^2}$ at the midpoints of our grid by interpolating $4\pi r^2 K e^{\phi/c^2} / (1+z)$ and differencing $T e^{\phi/c^2}$; as a result the divergence term in equation (5) is second-order and explicitly conserves flux. This procedure yields a set of coupled ordinary differential equations, which we then integrate using a semi-implicit extrapolation method (see Press et al. 1992, and references therein). Our calculation of C , K , ϵ_{nuc} , and ϵ_ν is described in the Appendix.

We used two different boundary conditions for the core. The first is to simply assume a constant temperature, which we fit to observations. The second is to match the inwards luminosity at the crust-core boundary to the neutrino emission from the core using a tabulated T_c - L_ν relation for different assumptions of the core neutrino emissivity. In this way,

TABLE 1
PARAMETERS FOR NUMERICAL INTEGRATIONS

quantity	unit	KS 1731–260	MXB 1659–29
\dot{M}	g s^{-1}	10^{17}	10^{17}
T_{core}^{∞}	10^7 K	4.6	2.6
outburst duration	yr	12.0	2.5
recurrence time	yr	100	21

we self-consistently solve for the core temperature appropriate for the assumed core physics rather than treat it as a free parameter. Unless the quiescent interval is long, we find that the core temperature is essentially constant over an outburst-quiescence cycle.

The boundary condition at the surface is more ambiguous. During an outburst, the temperature in the neutron star envelope is set by the burning of hydrogen and helium, and (possibly) fusion of light elements such as ^{12}C . Our code does not track this burning, and so we fix the temperature at $P/g = 10^{12} \text{ g cm}^{-2}$ at a fixed value T_b . This column is roughly where superburst ignition occurs, and should demarcate the bottom of the region containing light element, unstable reactions. Because our first goal is to fit the lightcurve, for now we do not set T_b to any expected value *a priori*, but rather leave it as an adjustable parameter.

During quiescence, we calculate the cooling flux at the top of the grid using a tabulated relation between T_{eff}^{∞} and the temperature obtained by integrating the steady-state thermal structure of the neutron star envelope (Brown et al. 2002). In these integrations, we fix the envelope to be pure ^4He down to a depth $P/g = 10^9 \text{ g cm}^{-2}$, with a layer of pure ^{56}Fe down to a depth $P/g = 10^{12} \text{ g cm}^{-2}$. The resulting relation (Fig. 1, *solid line*) resembles that of Gudmundsson et al. (1983, *dashed line*) at low T_{eff} , but trends towards the fully accreted model of Potekhin et al. (1997, *dotted line*) at higher T_{eff} . We also show the calculation of (Potekhin et al. 1997) for a light element envelope that is accreted to a density (*dot-dashed line*). Note that our boundary is not quite as deep as the one used by Gudmundsson et al. (1983) or Potekhin et al. (1997). For comparison, we therefore show (*thin black line*) our relation $T_b(T_{\text{eff}})$ when the bottom of the ^{56}Fe layer is taken at the same density as used by Gudmundsson et al. (1983) and Potekhin et al. (1997).

2.3. Numerical Results

We now describe our method for fitting the data, using MXB 1659–29 as an example. With the hydrostatic structure constructed (eqs. [2]–[4]), we use the surface gravity and redshift to tabulate $T_b(T_{\text{eff}}^{\infty})$, where T_b is the temperature at $y = y_{\text{top}}$. We set the core temperature from the last observation of MXB 1659–29 (Cackett et al. 2008). Although our code can follow the thermal evolution of the core, the change in temperature is not large unless the quiescent interval is $\sim 10^3$ yr, the core cooling timescale. We therefore found it more convenient to fix the core temperature at this value. Table 1 shows the parameters for the calculations—accretion rate, core temperature, outburst duration, and recurrence time—described in this section. In both cases, we used a neutron star with a mass $1.62 M_{\odot}$, radius 11.2 km, surface gravity $2.27 \times 10^{14} \text{ cm s}^{-2}$, and surface redshift 1.32.

We base the outburst and recurrence times on observations. KS 1731–260 was first discovered in August 1989 with *Mir/Kvant* (Sunyaev 1989) and went into quiescence in 2001

(Wijnands et al. 2001). Its recurrence time is unknown, although it has been quiescent since then. So long as the recurrence time is longer than the thermal relaxation time of the crust (as determined by Shternin et al. 2007 and confirmed here), our results are not sensitive to the recurrence time since we are using the core temperature as a parameter in our fit. MXB 1659–29 has had two outbursts since being discovered in 1976 (Lewin et al. 1976). It was initially detected with *SAS3* and *HEAO* through 1978; subsequent observations with a variety of instruments (see Wijnands et al. 2003, and references therein) failed to detect the source until it was detected in outburst again in 1999 (in ‘t Zand et al. 1999). This outburst was monitored with *RXTE/ASM* until the source went into quiescence in September 2001. We adopt an outburst duration of 2.5 yr and a recurrence time of 21 yr. For both sources we adopt an accretion rate $\dot{M} = 10^{17} \text{ g s}^{-1}$, which is consistent with recent estimates (Galloway et al. 2008, see § 3.2), for example from the X-ray luminosity using the relation for energy radiated by radially infalling material (see, e. g., Ayasli & Joss 1982) $\dot{M} = (1+z)L^{\infty}/c^2 z$. There is uncertainty in deriving the mass accretion rate from the source luminosity, and we shall explore the sensitivity of our conclusions to the assumed mass accretion rate in § 3.2.

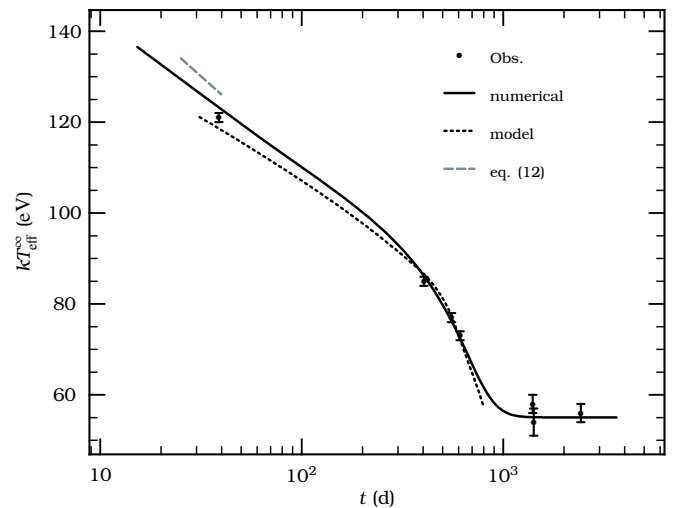


FIG. 2.— An example of a lightcurve that fits the observed cooling of MXB 1659–29. The numerical model is shown as a solid curve and has $Q_{\text{imp}} = 4.0$ and $T_b = 3.8 \times 10^8 \text{ K}$. The dotted curve shows the corresponding toy model lightcurve from §2.4, and we also show (*grey dashed line*) the slope given by eq. (12).

To generate a starting model, we first compute the thermal structure for a steadily accreting neutron star at the outburst accretion rate \dot{M} . We then turn on the time-dependent terms in equations (5)–(6). We run through several outburst/quiescent cycles, and then generate a quiescent lightcurve with finer time resolution. Because the recurrence time is unknown for KS 1731–260, we use in the code an arbitrary recurrence time of 100 yr; note that our results do not depend on the value of the recurrence time, however, since the core temperature is held fixed. The code stores snapshots of the temperature during this “high resolution” run so that the physical properties of the crust during its gloaming can be reconstructed.

Several runs with different values of Q_{imp} and T_b were then made, adjusting the chosen values to provide a good fit by eye to the lightcurve. Although there is no physical reason why Q_{imp} should be the same value throughout the crust, there are

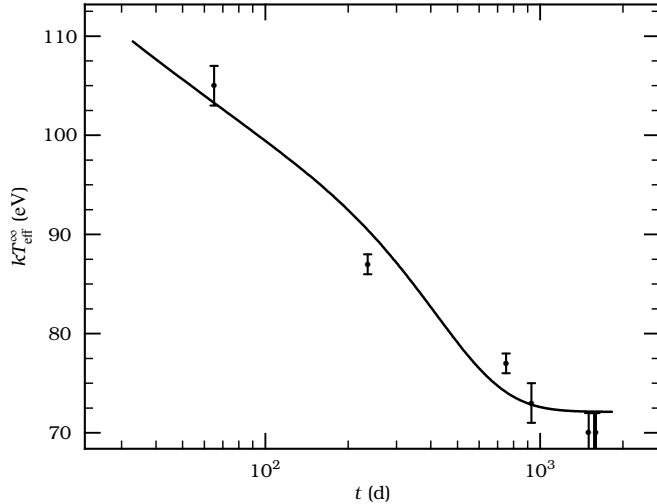


FIG. 3.— A model lightcurve for KS 1731–260, with $Q_{\text{imp}} = 1.5$ and $T_b = 2.5 \times 10^8$ K.

no reliable calculations of how Q_{imp} would evolve with depth, and we therefore choose to set Q_{imp} to a constant. Indeed, we shall show (§ 2.4) that it is really the value of Q_{imp} in the inner crust that is important for determining the lightcurve. Figure 2 shows a fit for MXB 1659–29, with $Q_{\text{imp}} = 4.0$ and $T_b = 3.8 \times 10^8$ K. The lightcurve is a broken power law with a break at $t \approx 300$ d, going to a constant at late times.

Repeating this procedure for KS 1731–260, we find an acceptable fit with $Q_{\text{imp}} = 1.5$, $T_b = 2.5 \times 10^8$ K, as shown in Fig. 3. Note that the errors on the temperature given by Cackett et al. (2006) are (erroneously) stated to be 1- σ errors, but are in fact 90% confidence limits (Cackett et al. 2008). We show 1- σ errors in all figures in this paper. For the observations of MXB 1659–29 we use the published 1- σ errors (Cackett et al. 2008); for the observations of KS 1731–260 we assume a Gaussian distribution to adjust the published 90% confidence limits (Cackett et al. 2006) to 1- σ errors.

2.4. Simple understanding of the lightcurve

We now describe a simple model that accurately reproduces the lightcurve from the time-dependent calculation, and reveals the basic physics underlying the lightcurve. This will allow us to understand the effect of different parameters on the lightcurve. A similar approach has been applied to lightcurves of white dwarfs cooling following a dwarf nova (Piro, Aras, & Bildsten 2005), and the early phase of superburst lightcurves (Cumming et al. 2006, Appendix A).

We first note that during the long outbursts of MXB 1659–29 and KS 1731–260, the crust temperature profile is very close to the thermal steady-state profile at the outburst accretion rate. This is shown in Fig. 4 for MXB 1659–29, in which we compare the temperature at the end of the outburst of MXB 1659–29 in our numerical calculations (*top panel, dotted line*) with the temperature profile of a steady-state calculation at the outburst accretion rate (*top panel, dashed line*). The largest difference (Fig. 4, *bottom panel*), in the inner crust where the strongest heat sources lie, is only 4% percent. Therefore a good approximation to the initial temperature profile for the cooling is the steady-state profile. This is an even better approximation for KS 1731–260, which had a longer outburst than MXB 1659–29. Our calculation is therefore different from that of Ushomirsky & Rutledge (2001), who injected the

entire heat deposition of the outburst at once.

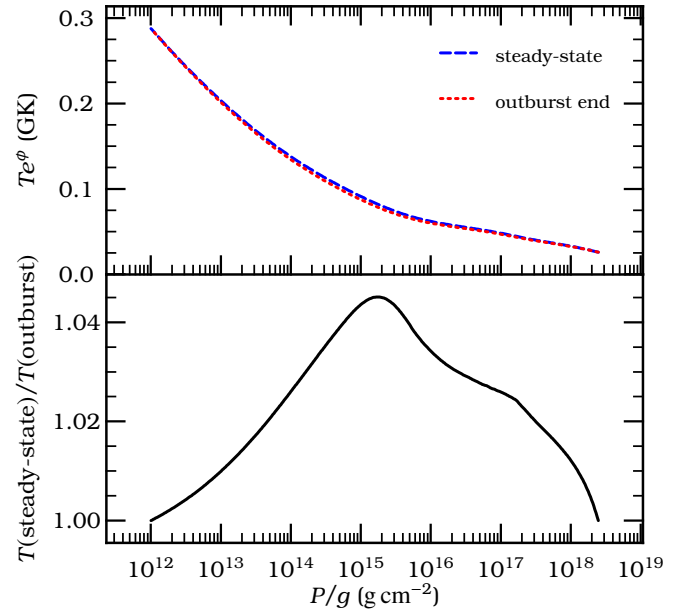


FIG. 4.— (*Top panel*) Temperature in the crust of MXB 1659–29 at the end of a 2.5 yr outburst (*dotted line*) and that of a neutron star in thermal steady-state accreting at the outburst accretion rate (*dashed line*). Note that the core temperature and the temperature at a column $y_{\text{top}} = 10^{12}$ g cm $^{-2}$ are fixed. (*Bottom panel*) Ratio of the steady-state temperature to that at the outburst end.

Starting with the initial temperature profile, we can understand the evolution of the cooling layer and the resulting lightcurve by noting that at a given depth, the thermal evolution occurs on the characteristic thermal timescale associated with that depth. This is illustrated in the middle panel of Figure 5, which shows snapshots of the temperature profile of the crust as it cools during quiescence. At a given time, the temperature profile has two parts: the inner layers have not yet started to cool and still have the temperature profile corresponding to the initial condition (the steady state profile during outburst); the outer layers have relaxed thermally and the temperature profile there corresponds to a constant outwards flux. The transition occurs at a depth where the thermal time at that depth is equal to the current time. In the bottom panel of Figure 5, we show the thermal time as a function of depth, where we calculate the thermal time from the surface following Henyey & L’Ecuyer (1969),

$$\tau \equiv \frac{1}{4} \left[\int_0^z \left(\frac{\rho C_P}{K} \right)^{1/2} dz' \right]^2. \quad (7)$$

where ρ is the density, C_P the specific heat, and K the thermal conductivity. In the top panel of Figure 5 we show the temperature profiles as a function of the thermal time. This shows directly that the deviation of each of the dashed temperature profiles away from the initial temperature profile occurs at a depth where the thermal time is approximately equal to the time since cooling began.

The temperature of the inner crust is also affected by conduction of heat into the core. We show the timescale for thermal diffusion into the core in Figure 5 (*bottom panel, dotted line*). The two thermal times intersect at a depth ($P/g \sim 10^{16}$ g cm $^{-2}$) where the thermal diffusion time is ≈ 400 d. After this point the temperature in the inner crust

drops markedly (*top panel*).

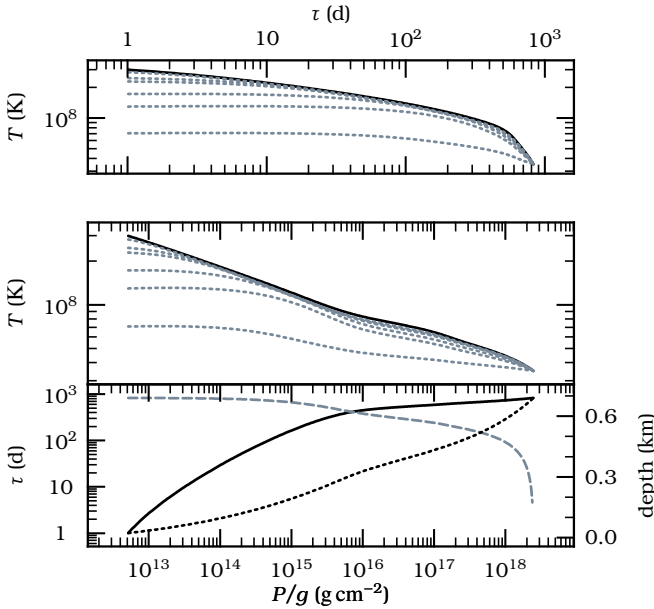


FIG. 5.— Illustration of the cooling behavior of our analytical model. The bottom panel shows the thermal diffusion time, as a function of P/g , to the surface (eq. [9]; *solid line*) and to the core (*grey dashed line*), as well as the depth from the surface (*dotted black line*, right axis). The middle panel shows the temperature as a function of P/g . In the top panel, we plot the temperature (*solid line*) against τ at the start of the quiescent phase. Subsequent “snapshots” of the temperature in the crust (*grey dotted lines*) at $t = 3.1, 10, 31, 107, 305,$ and 504 d plotted against τ (*top panel*) and P/g (*middle panel*).

This understanding suggests a simple model of the lightcurve. We start with the initial temperature profile set by the steady-state profile at the outburst accretion rate. Then, for each time t , we locate the depth at which $\tau = t$. We then find the outwards flux in a constant flux solution that has a temperature equal to the initial temperature at the depth where $t = \tau$. This value of flux is the flux emerging from the surface at time t . The dotted curve in Figure 2 shows a lightcurve calculated in this way, using the same parameters Q_{imp} , T_b , and T_c as the numerical model. The simple model shows excellent agreement with the numerical model.

The origin of the broken power law nature of the lightcurve lies in the change in slope of the thermal time with depth that occurs close to neutron drip (see the lower panel of Fig. 5; neutron drip occurs at $P/g \approx 5 \times 10^{15} \text{ g cm}^{-2}$). The decrease in slope is primarily due to the suppression of C_p in the inner crust, shown in Figure 6. The ion contribution to the specific heat (*bottom panel*, *dotted line*) decreases on going to higher densities roughly as $(T/\Theta_D)^3$, where the Debye temperature $\Theta_D \propto \Theta_p = (\hbar/k_B) [4\pi Z^2 e^2 n_{\text{ion}} / (Am_u)]^{1/2}$, the plasma temperature of the ions. We assume that the neutrons in the inner crust are superfluid, in which case they have a negligible contribution to the heat capacity (Fig. 6, *bottom panel*, *dot-dashed line*). The thermal time also depends on the thermal conductivity, which changes from being set by phonon scattering in the outer crust to impurity scattering in the inner crust (*top panel*, *dashed line*). Electron-electron scattering, although included in our calculations, is not a significant component of the total thermal conductivity (Shternin et al. 2007), and we do not show it in Fig. 6. The slight step in the ion specific heat at $P/g \lesssim 10^{13} \text{ g cm}^{-2}$ (Fig. 6, *bottom panel*) is caused by the

liquid-solid transition in the crust. Our code does not follow the crystallization front and hence does not include the latent heat. The depth where crystallization occurs is so shallow, however, that this omission does not appreciably affect the lightcurve, unlike the case for the cooling of white dwarf stars (see Chabrier 1999; Hansen 2004, and references therein). We note that observations taken shortly ($\lesssim 10$ d) after the end of the outburst could potentially detect the effect of the latent heat; this would provide an independent constraint on the temperature in the crust and a check on the value of the plasma parameter Γ at which the ions crystallize (see Appendix A.1).

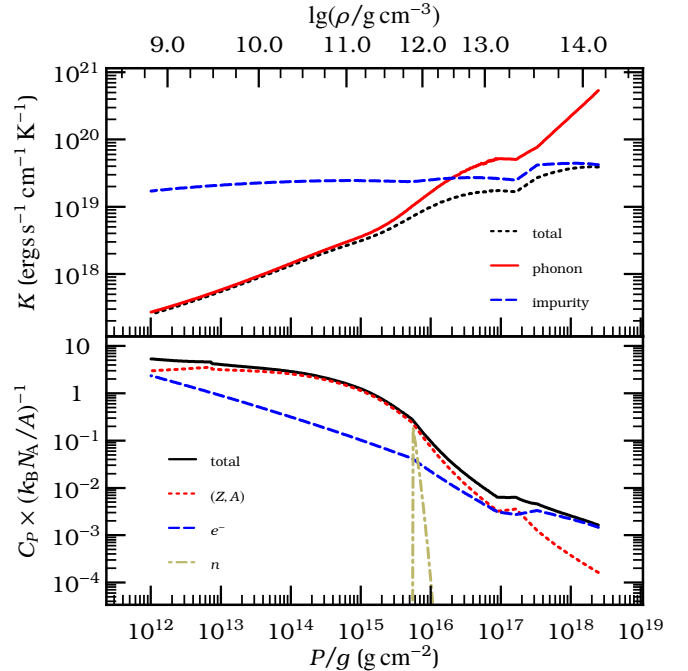


FIG. 6.— Physical quantities setting the thermal diffusion time (cf. eq. [9]). The top panel shows the total thermal conductivity (*dotted line*), and the conductivity resulting from electron-phonon (*solid line*) and electron-impurity (*dashed line*) scattering. These quantities are computed for the temperature at the end of the outburst for the run corresponding to MXB 1659–29. The bottom panel displays the specific heat (*solid line*), in units of $k_B N_A / A$, and the contributions from ions (*dotted line*), electrons (*dashed line*), and neutrons (*dot-dashed line*). The slight step in C_p (*bottom panel*) at $P/g \lesssim 10^{13} \text{ g cm}^{-2}$ is where the ions crystallize. The top axis of the plot indicates the density as a function of P/g . The scale is not linear because of the change in the effective polytropic index in the inner crust.

With some approximations, the same arguments allow us to make an analytic approximation to the lightcurve. The slope of the cooling curve can be written

$$\frac{d \ln T_{\text{eff}}^{\infty}}{d \ln t} = \left(\frac{d \ln T_{\text{eff}}^{\infty}}{d \ln T} \right) \left(\frac{d \ln T}{d \ln y} \right) \left(\frac{d \ln y}{d \ln \tau} \right). \quad (8)$$

The first factor on the right hand side is the slope of the $T_{\text{eff}} - T$ relation, $d \ln T_{\text{eff}}^{\infty} / d \ln T \approx 0.45 - 0.63$ (Fig. 1). The second factor is the temperature gradient in the initial model. The third factor is the dependence of thermal time with column depth. We can obtain this analytically by noting that during the early part of the lightcurve, when the cooling wave is in the outer crust, we can approximate the heat capacity as $C_p \approx 3k_B / (Am_u)$ the classical heat capacity of a lattice, and use an approximate expression for the phonon conductivity (see eq. [A3]–[A4]). Inserting these expressions into the ex-

pression for τ (eq. [7]), we find²

$$\tau \approx 34 \text{ d} \cdot y_{14}^{3/4} \left(\frac{2.3}{g_{14}} \right)^{5/4} \left(\frac{Y_e}{0.5} \right) \left(\frac{60}{A} \right), \quad (9)$$

where $g_{14} = g/10^{14} \text{ cm s}^{-2}$, giving $d \ln \tau / d \ln y = 3/4$.

A measurement of the slope during the early part of the lightcurve directly measures, therefore, the temperature gradient in the outer crust at the end of the outburst,

$$\frac{d \ln T}{d \ln y} \approx \frac{15}{11} \frac{d \ln T_{\text{eff}}^{\infty}}{d \ln t}. \quad (10)$$

The fact that the effective temperature is decreasing with time, implies that temperature decreases with depth in the crust: the temperature profile in the outer crust is inverted during outburst. If the temperature increased with depth in the crust, equation (10) implies that we would see an increasing temperature with time, and this can in fact be seen in the numerical models of Rutledge et al. (2002, see their Fig. 3).

A different way to write equation (10) is in terms of the inwards flux in the outer crust, since the flux determines the temperature gradient. We write the flux as $F = -KdT/dr$ and use the expression for K , eqs. (A3)–(A4) to obtain

$$\frac{d \ln T}{d \ln y} = 0.04 \left(\frac{F}{10^{21} \text{ ergs s}^{-1} \text{ cm}^{-2}} \right) \left(\frac{Y_e}{0.5} \right) \left(\frac{2.3}{g_{14}} \right)^{5/4} y_{14}^{-1/4} T_8^{-1}. \quad (11)$$

giving

$$\frac{d \ln T_{\text{eff}}^{\infty}}{d \ln t} = 0.03 \left(\frac{F}{10^{21} \text{ ergs s}^{-1} \text{ cm}^{-2}} \right), \quad (12)$$

where we have suppressed the other factors from equation (11) and we use $d \ln T_{\text{eff}}^{\infty} / d \ln T = 0.55$. As an example, we plot a line representing this slope in Fig. 2 (*grey dashed line*), but using $d \ln T_{\text{eff}}^{\infty} / d \ln T = 0.45$, as appropriate at this T_{eff}^{∞} . The slope of the early-time power law directly measures the flux in the rust.

Our inference that the temperature gradient in the crust is inverted, i. e., the temperature decreases with depth, also implies that an inward-directed heat flux enters the crust from the top. To show how this is critical for the early decay, Figure 7 compares our original fit (*dotted line*) for KS 1731–260 with runs in which we do not hold the temperature at the top of the crust fixed, but rather use the same boundary condition (see Fig. 1) during both outburst and quiescence (*dashed and solid lines*). We first changed only the condition on T_b , while holding all other parameters fixed (*dashed line*). Although the break in the lightcurve occurs on the same timescale, the calculation with deep heating only is too faint to match observations. We then increased the accretion rate to $\dot{M} = 3.5 \times 10^{17} \text{ g s}^{-1}$, which gives a crust heating rate comparable to that used by Shternin et al. (2007). Because the higher temperature decreases the thermal conductivity, we set $Q_{\text{imp}} = 0$ to compensate. The resulting solution (*solid line*) gives a better fit, although its early time behavior still undershoots the first observation. For both latter cases (*dashed and solid lines*), the temperature profile is inverted for $P/g \gtrsim 10^{13} \text{ g cm}^{-2}$; that is, most of the heat produced in the outer crust during outburst is conducted inward. As a re-

² In principle, we could include the dependence of Y_e on y (eq. [A2]), but for simplicity we shall leave it free in this formula. This expression agrees well with our numerical calculations (Fig. 5, *bottom panel*).

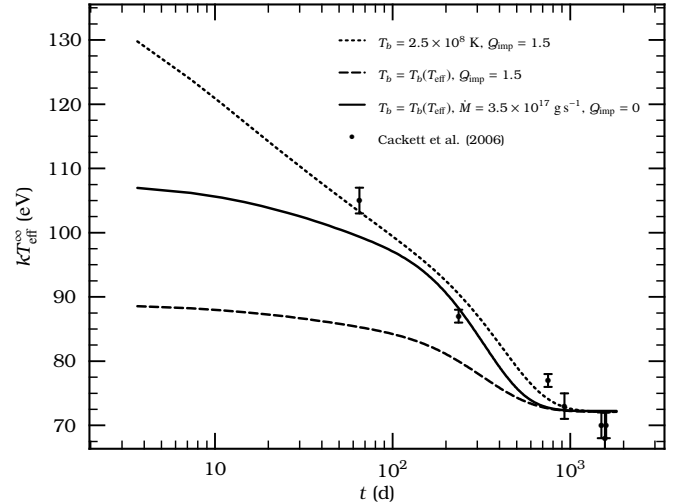


FIG. 7.— Our fit to the lightcurve for KS 1731–260 (*dotted line*) compared to calculations for which the outer boundary condition during outburst was replaced with the same $T_b(T_{\text{eff}})$ relation used during quiescence (*dashed, solid lines*). For the case where other parameters were held fixed (*dashed line*), the lightcurve falls markedly below the observed values. When the outburst accretion rate is increased to $3.5 \times 10^{17} \text{ g s}^{-1}$ and the impurity parameter decreased to $Q_{\text{imp}} = 0$ (*solid line*) a better agreement is found with the observed lightcurve. A clear distinction between these scenarios could be observed during the first fortnight of quiescence.

sult, T_{eff}^{∞} is decreasing with time starting a few days after the end of outburst in these cases.

As noted by Shternin et al. (2007), the observed lightcurve of KS 1731–260 can be explained without recourse to an inward-directed heat flux provided that \dot{M} is larger than the value we assume in this paper (cf. Fig. 7). We have made the same comparison for MXB 1659–29 (Fig. 8): we used the same $T_b(T_{\text{eff}})$ relation during both outburst and quiescence, and then increased \dot{M} while decreasing Q_{imp} . In addition to our best-fit solution with fixed T_b (*dotted line*), we show the case for $\dot{M} = 5 \times 10^{17} \text{ g s}^{-1}$ and $Q_{\text{imp}} = 1$ (*dashed line*) and $\dot{M} = 9 \times 10^{17} \text{ g s}^{-1}$ and $Q_{\text{imp}} = 0$. Without a fixed T_b during outburst (or equivalently a sizeable inward-directed heat flux in the shallow outer crust), we do not find an acceptable numerical solution consistent with the observed MXB 1659–29 lightcurve.

To illustrate this point, we computed, using equation (12), the required flux necessary to match the observed power-law slope between the first two observations. For KS 1731–260 the first two observations imply a flux of $0.7 \text{ MeV}/m_u$ for $\dot{M} = 10^{17} \text{ g s}^{-1}$. For MXB 1659–29, the flux required to match the observed power-law slope is $0.8 \text{ MeV}/m_u$ for $\dot{M} = 10^{17} \text{ g s}^{-1}$. Our numerical solutions are consistent with this estimate: our numerical model of the KS 1731–260 lightcurve (Fig. 3) has a local inward flux of $0.5 \text{ MeV}/m_u$, while our model of the MXB 1659–29 lightcurve (Fig. 2) has $1.1 \text{ MeV}/m_u$. This value of the flux is well above the estimates available from electron captures (Gupta et al. 2007). Moreover, this flux would have to emanate from a depth for which the thermal time is less than the time of the first observation, which is $P/g \lesssim 2 \times 10^{14} \text{ g cm}^{-2}$, corresponding to $\rho \lesssim 3 \times 10^{10} \text{ g cm}^{-3}$. This is a lower density than that of many crust electron captures (Gupta et al. 2007; Haensel & Zdunik 2008) and even that of light element pycnonuclear reactions, such as ^{24}O (Horowitz et al. 2008b). Hence, although a larger \dot{M} reduces the total amount of heating per nucleon required, matching the first data point is still difficult. Observations of

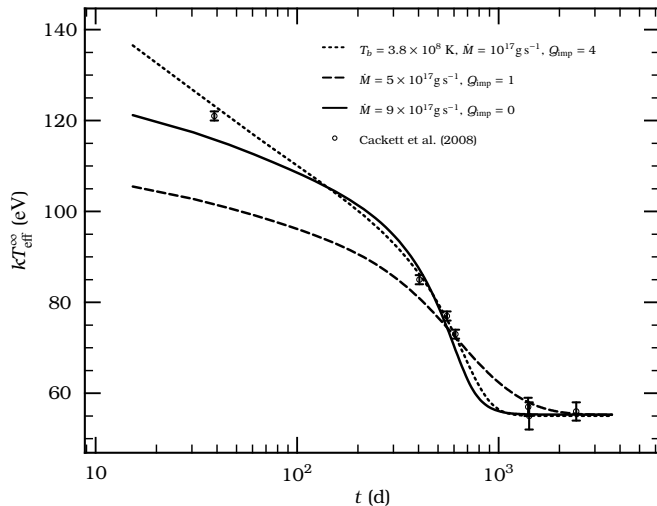


Fig. 8.— A comparison between the observed lightcurve of MXB 1659–29 and several trial numerical solutions: 1) our best-fit solution (dotted line; cf. Fig. 2) with $T_b = 3.8 \times 10^8$ K and $\dot{M} = 10^{17}$ g s $^{-1}$; a solution with $\dot{M} = 5 \times 10^{17}$ g s $^{-1}$, $Q_{\text{imp}} = 1$, and $T_b = T_b(T_{\text{eff}})$ (dashed line); and a solution with $\dot{M} = 9 \times 10^{17}$ g s $^{-1}$, $Q_{\text{imp}} = 0$, and $T_b = T_b(T_{\text{eff}})$.

both sources are too sparse on timescales $\lesssim 10^2$ d, however, to draw firmer conclusions about the existence and nature of this heating. Observations occurring within the first two weeks after the outburst ends are critical for constraining the depth and strength of heat sources in the outer crust.

3. CONSTRAINTS ON THE MODEL PARAMETERS

In Figures 2 and 3, we show models that fit the data well for MXB 1659–29 and KS 1731–260. We now address the uncertainties in the fitted model parameters. The cooling models have a range of physics input. To allow us to investigate the full range of parameter space, we adopt the simplified model of the cooling curves described in §2.4 as it allows us to rapidly generate a lightcurve without running the full time-dependent simulation.

To calculate the constraints on model parameters, we adopt a Markov Chain Monte Carlo (MCMC) method, using the Metropolis-Hastings algorithm to generate a sequence of samples from the posterior probability distributions (e. g., Gregory 2005). Although we have a small number of parameters which would allow a grid search of the chi-squared space, we prefer the MCMC method for its simplicity in implementation and generating marginalized probability distributions. We run the chains multiple times from different starting points to check the convergence and robustness of the resulting probability distributions. Typically, we find that $\sim 10^4$ samples are adequate, although we have run the chains longer to check convergence.

Although the simplified model lightcurves agree well with the numerical results (as shown for a specific example in Figure 2), the agreement is not exact, and as a result the best-fit parameters derived from the two models are different. For example, whereas the best fit lightcurve, for MXB 1659–29, from the time-dependent simulation has $Q_{\text{imp}} = 4$ (Fig. 2), the simplified model gives a best fit value $Q_{\text{imp}} = 2$. In this section our focus is, however, on how well we can constrain the main parameters of the model, and how each of these parameters changes the lightcurve, rather than the best-fit values. By running a sample of comparison models, we have checked that the uncertainties in the parameters derived from the simplified model and time-dependent simulations are similar.

3.1. Constraints for a given hydrostatic structure

For a given hydrostatic structure, which is set by the neutron star mass and radius, the three main parameters that affect the lightcurves are the temperatures at the top of the crust T_b , the core temperature T_c , and the impurity parameter Q_{imp} . We assume for now that the accretion rate, which determines the overall heating rate in the crust (see Appendix), is determined from the observed X-ray luminosity. We fix the neutron star mass $M = 1.6 M_{\odot}$ and radius $R = 11.2$ km, and the outburst accretion rate $\dot{M} = 10^{17}$ g s $^{-1}$ for both sources. These values match the parameters used in the time-dependent code to calculate the models shown in Figures 2 and 3. The corresponding redshift factor is $1 + z = 1.32$ and gravity is $g_{14} = 2.3$.

Figure 9 shows the resulting probability distributions for Q_{imp} , T_c^{∞} and T_b . The values of T_c^{∞} and T_b are well-constrained in each case. These two temperatures are constrained by the need to match the first and last data points in each set of observations. The first data point gives a snapshot of the temperature near the top of the crust (thermal time of tens of days), whereas the last point gives a measurement of the core temperature (we find that the lightcurve has leveled off in both sources in our models).

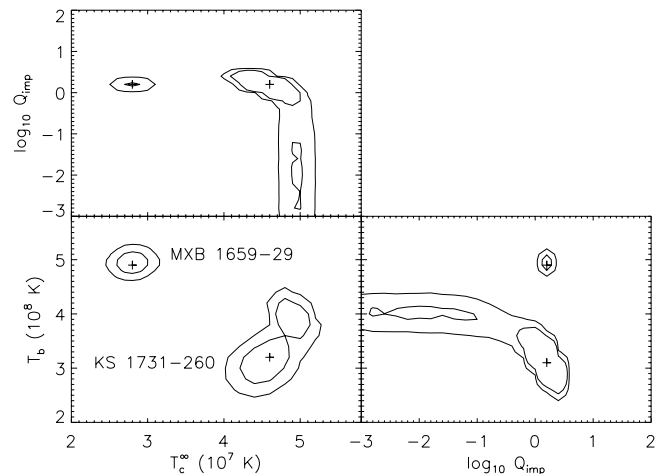


Fig. 9.— Probability densities for Q_{imp} , T_c^{∞} and T_b for MXB 1659–29 and KS 1731–260. The peak of the probability distribution is marked by a cross, and the contours show the 68% and 95% confidence intervals. The prior probability for Q_{imp} is taken to be uniform in log from $Q_{\text{imp}} = 10^{-3}$ to 10^2 . For each source, we fix the outburst accretion rate at $\dot{M} = 10^{17}$ g s $^{-1}$ and the neutron star mass and radius at $M = 1.6 M_{\odot}$ and $R = 11.2$ km.

The impurity parameter Q_{imp} is very tightly constrained in MXB 1659–29. To understand why this is the case, we show in Figure 10 several lightcurves from our time-dependent simulations for MXB 1659–29 with different values of Q_{imp} . In the left panel, we keep all other parameters fixed as we vary Q_{imp} ; in the right panel, we adjust T_b to match the first data point as we vary Q_{imp} . The effect of increasing Q_{imp} is to delay the cooling. This can be understood in terms of the initial temperature profile at the end of the outburst. When the crust has a larger impurity level, the inner crust must be hotter to be able to conduct the heat released in the crust into the core. This increase in the inner crust temperature leads to a hotter outer crust, with a shallower temperature gradient, giving a lightcurve that falls less quickly.

As Figure 9 shows, the correlations between the fitted parameters are such that larger Q_{imp} values lead to lower values of T_c and T_b , i.e. to compensate for the delayed cooling due to

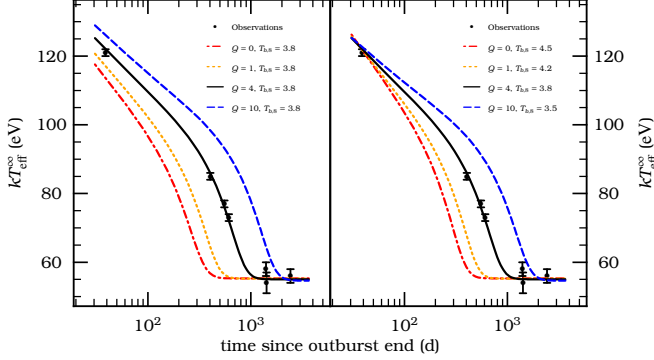


FIG. 10.— Lightcurves of MXB 1659–29, for different choices of the impurity parameter Q_{imp} in the crust. In both case, we show the best fit model (solid line). The other solutions have $Q_{\text{imp}} = 0$ (dot-dashed line), 1 (dotted line), and 10 (dashed line). The left-hand panel shows the case for which all other parameters are held constant; in the right-hand panel the temperature at a column $\nu_{\text{top}} = 10^{12} \text{ g cm}^{-3}$ was adjusted so that all solutions matched the first data point.

increase in Q_{imp} , the overall temperature scale set by T_c and T_b decreases. In KS 1731–260, the probability distribution of Q_{imp} has a peak at a similar value to MXB 1659–29, but with a long tail to small values of Q_{imp} . In fact, as can be seen in Figure 11, the fits are not sensitive to the impurity parameter for $Q_{\text{imp}} \lesssim 1$, which results in a flat probability distribution in $\log Q_{\text{imp}}$, reflecting the assumed prior. For both sources, Q_{imp} values larger than 10 are ruled out.

For MXB 1659–29, we have used the temperatures derived by Cackett et al. (2008) assuming a distance to the source of 10 kpc. In that paper, spectral models for different distances $d = 5$ and 13 kpc are considered, which leads to a systematic decrease or increase in the effective temperatures by 10–20%. The reason that the fitted effective temperatures depend on distance is that the peak of the thermal spectrum lies outside the X-ray band, making the fitted temperature sensitive to the overall luminosity scale. To investigate the effect of such systematic variations, we have calculated the constraints on the models with the effective temperatures for MXB 1659–29 all decreased or increased by 20%. The effect is to change the central value of each distribution by up to 50%, with the width staying about the same. The conclusion that Q_{imp} is of order unity is unaffected by these systematic variations.

3.2. The accretion rate or overall heating rate in the crust

The accretion rate \dot{M} sets the overall amount of heating in the crust during the outburst. There are uncertainties in deriving \dot{M} from the observed X-ray luminosity, and in addition, the amount of heating in the crust may differ from the 1.7 MeV per nucleon that we assume in our calculation (see Appendix for details). The calculations so far have taken a fixed accretion rate $\dot{M} = 10^{17} \text{ g s}^{-1}$. Instead, we now calculate the constraints on \dot{M} assuming a uniform prior probability for \dot{M} between 0 (i.e. no deep heating) and 10^{18} g s^{-1} (ten times our fiducial rate). The results are shown in Figure 11, in which we give the derived joint probability distribution for \dot{M} and Q_{imp} for each source. The temperatures T_b and T_c are not sensitive to variations in \dot{M} , since they are essentially fixed by the first and last observed values of $T_{\text{eff}}^{\text{oo}}$.

For both sources, we find an anti-correlation between \dot{M} and Q_{imp} in the best-fitting solutions. The explanation for the anti-correlation is that an increased \dot{M} gives an increased heating rate, making the inner crust hotter. To compensate for this, Q_{imp} must decrease, cooling the inner crust by making it eas-

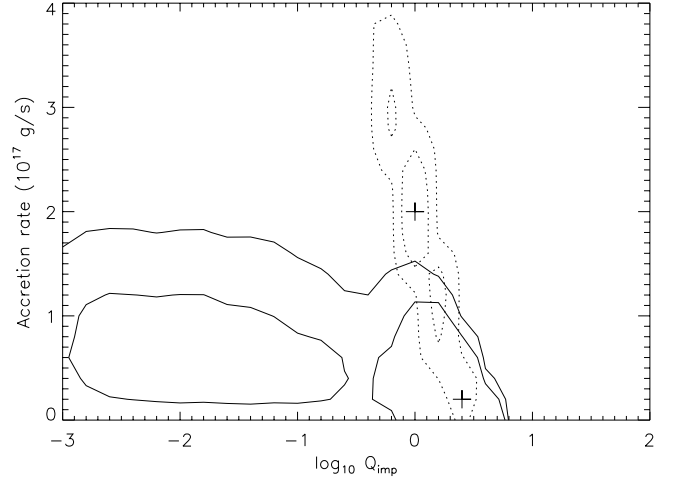


FIG. 11.— The joint probability distribution of Q_{imp} and \dot{M} for MXB 1659–29 (dotted contours) and KS 1731–260 (solid contours). In each case, the peak of the probability distribution is indicated by a cross; the two contours enclose 68% and 95% of the probability.

ier for heat to be conducted into the core.

The values of \dot{M} derived from the cooling curves match well with the accretion rates derived from observations of the persistent X-ray luminosity during outburst. For MXB 1659–29, the range of flux observed during the outburst was $\approx (0.4\text{--}1) \times 10^{-9} \text{ ergs s}^{-1} \text{ cm}^{-2}$ (2.5–25 keV) (Galloway et al. 2008). Galloway et al. (2008) found a distance of 12 ± 3 kpc for this source, assuming that the peak flux of photospheric radius expansion bursts corresponds to the pure helium Eddington luminosity. Taking this distance and assuming a bolometric correction of a factor of 2, typical for these sources, gives $\dot{M} \approx (0.7\text{--}1.8) \times 10^{17} \text{ erg s}^{-1}$. The agreement with the constraints from the cooling curve is good, although lower than the maximum of the probability distribution for \dot{M} .

For KS 1731–260, Galloway et al. (2008) give a range of bolometric flux $1.6\text{--}10 \times 10^{-9} \text{ erg cm}^{-2} \text{ s}^{-1}$, which for their distance 7.2 ± 1 kpc gives a range of accretion rates during outburst of $0.5\text{--}3 \times 10^{17} \text{ g s}^{-1}$. A separate check on this value is that at a flux level of $2.1 \times 10^{-9} \text{ erg cm}^{-2} \text{ s}^{-1}$, a very regular sequence of X-ray bursts was seen, similar to the source GS 1826-24, which is known for being a very regular burster. Assuming an ignition mass of 10^{21} g for these regular bursts, which had a recurrence time of 2.59 ± 0.06 h, we find $\dot{M} = 1.1 \times 10^{17} \text{ g s}^{-1}$, consistent with the X-ray flux. During the final $\gtrsim 1$ year of the outburst, the flux was in the lower end of the flux range quoted earlier, so we expect the relevant value for the crust heating at the end of the outburst to be $\lesssim 10^{17} \text{ g s}^{-1}$, in good agreement with Figure 11.

An interesting aspect of our results is that both sources allow solutions with low accretion rates much smaller than the accretion rates derived from the X-ray observations. Assuming that the observed accretion rate is within a factor of two of the true accretion rate onto the neutron star, this means that both cooling curves are consistent with a much lower amount of deep crustal heating than assumed in our models. In these models, however, a lower level of deep crustal heating from reactions in the crust is compensated by a larger inward heat flux from the neutron star ocean, because T_b is held fixed. In reality, the physics of the implied, unspecified heat source in the neutron star ocean that supplies this flux also depends on the accretion rate.

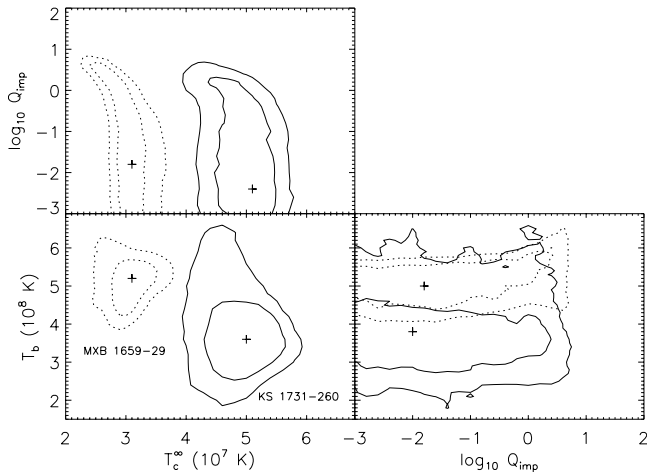


FIG. 12.— Constraints on T_c^∞ , T_b , and Q_{imp} , as in Figure 9, but now including variations in M , R , and \dot{M} .

3.3. Effect of varying neutron star mass and radius

We now include the uncertainty in all six parameters of the model. The prior probabilities for T_c^∞ , T_b , Q_{imp} , and \dot{M} are as described previously. In addition, we assume a uniform prior in the range 8–16 km for R and 1.1 to 2.5 M_\odot for M . The fit for T_{eff}^∞ used a fixed $M = 1.4 M_\odot$ and $R = 10$ km (Cackett et al. 2006, 2008) because the quality of the data is insufficient to constrain these parameters independently; therefore, the constraints we derive should be considered indicative. The resulting constraints on T_c^∞ , T_b , and Q_{imp} are shown in Figure 12. This Figure should be compared with Figure 9, for which M , R , and \dot{M} were assumed to be known. Including the uncertainty in the extra parameters broadens the probability distributions of T_c^∞ , T_b and Q_{imp} . The largest effect is on the probability distribution of Q_{imp} . For example, the constraint on Q_{imp} is considerably relaxed for MXB 1659–29. For both sources, however, Q_{imp} values greater than several are ruled out even with the additional parameters included. The central values of T_c^∞ and T_b are similar to the values previously derived.

The sensitivity of the derived value of Q_{imp} on M and R is illustrated for MXB 1659–29 in Figure 13 (we see the same effect for the KS 1731–260 data). We show the derived probability distribution for Q_{imp} for three different choices of neutron star mass and radius. In each case, we keep the accretion rate fixed at our fiducial value $\dot{M} = 10^{17} \text{ g s}^{-1}$. The allowed values of Q_{imp} increase with increasing surface gravity. This can be understood by considering the thermal time from a given density to the surface, which depends on the thickness of the layer and therefore varies with surface gravity (Lattimer et al. 1994). Rewriting the integral for the thermal time, equation (9), as an integral over pressure gives $\tau^\infty \propto (1+z)/g^2 \propto R^4 M^{-2} (1+z)^{-1}$. An increase in surface gravity shortens the cooling time, and Q_{imp} must increase to bring it back into agreement with the observed value.

Figure 14 shows the joint probability density for M and R for each source. Although M and R are only weakly constrained, we see that the best-fitting values of M and R are correlated. The mass and radius enter the calculation of the lightcurve in several places besides the thermal time τ^∞ . The relation between crust temperature and T_{eff}^∞ depends on the surface gravity; for a fixed crust temperature, $T_{\text{eff}}^\infty \propto g^{1/4}/(1+z)$. The initial temperature profile also changes

with gravity. Using the Newtonian equations for the steady-state thermal profile, we see that $dT/dP = (1/g)(3\kappa F/4acT^3)$, $dF/dP = -\epsilon/g$, so that the increase in flux due to the deep heating is smaller by a factor g , and the change in temperature for a given flux is smaller by a factor g . The combination of these different effects results in the observed correlation between the best fitting values of M and R . By inspection we find that the slope of the relation is well-described by $g \propto (1+z)^3$.

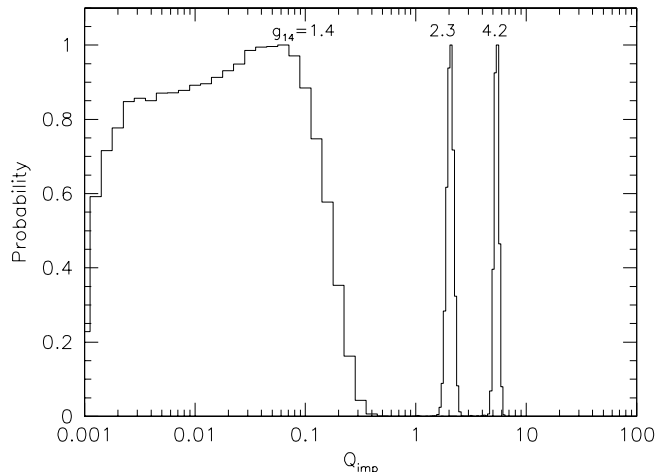


FIG. 13.— The probability distribution of Q_{imp} derived for MXB 1659–29, for three different choices of neutron star mass and radii. Left to right, in order of increasing surface gravity, they are (i) $M = 1.4 M_\odot$, $R = 13$ km, $g_{14} = 1.4$, $1+z = 1.21$ (ii) $M = 1.6 M_\odot$, $R = 11.2$ km, $g_{14} = 2.3$, $1+z = 1.32$ and (iii) $M = 2 M_\odot$, $R = 10$ km, $g_{14} = 4.2$, $1+z = 1.57$. In each case, the accretion rate is fixed at our fiducial value $\dot{M} = 10^{17} \text{ g s}^{-1}$. Note that the spectral fits used to obtain T_{eff}^∞ assume a fixed value of $M = 1.4 M_\odot$ and $R = 10$ km.

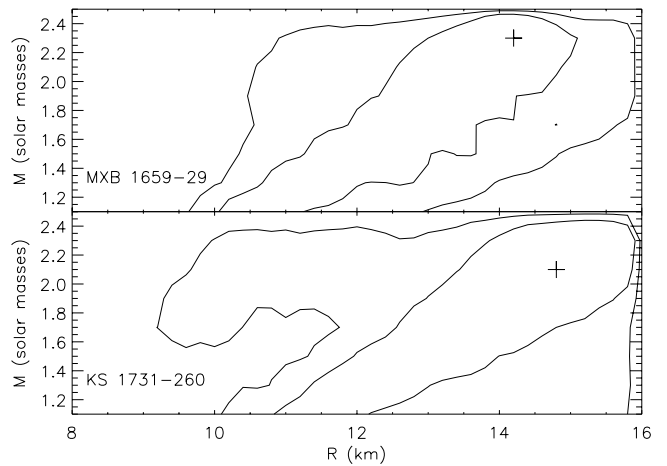


FIG. 14.— Constraint on the neutron star mass and radius. We assume a constant prior in mass between 1.1 and 2.5 M_\odot and in radius between 8 and 16 km. The peak of the probability distribution is marked with a cross, and the contours enclose 68% and 95% of the probability. Note that the spectral fits used to obtain T_{eff}^∞ assume a fixed value of $M = 1.4 M_\odot$ and $R = 10$ km.

4. DISCUSSION AND CONCLUSIONS

We have presented numerical simulations of the cooling of the neutron star crust in both KS 1731–260 and MXB 1659–29 following the end of long accretion outbursts. Our main results are as follows.

1. The lightcurve of a cooling crust is a broken power-law going to a constant at late times. The luminosity at late times is set by the neutron star core temperature. The slope of the early part of the lightcurve provides a direct measure of the flux in the outer crust during outburst (eq. [12]). The time of the break is set by the transition from a classical to quantum crystal, close to neutron drip. The good fit of our models to the data suggests that the neutrons in the inner crust do not contribute significantly to the heat capacity, as expected if they were superfluid. Observations of cooling quiescent neutron stars thus provide new evidence for the existence of a neutron superfluid throughout the inner crust.
2. As our models show, the observations to date probe the thermal relaxation timescale of the inner crust. The cooling timescale increases with increasing Q_{imp} , potentially giving a tight constraint on this parameter. The fits to the lightcurves of MXB 1659–29 and KS 1731–260 both require $Q_{\text{imp}} < 10$, in agreement with the result of Shternin et al. (2007) for KS 1731–260. For our fiducial model, which has neutron star parameters $M = 1.6 M_{\odot}$, $R = 11.2$ km, and outburst accretion rate $\dot{M} = 10^{17} \text{ g s}^{-1}$, the best fit values are $Q_{\text{imp}} = 4$ for MXB 1659–29, and $Q_{\text{imp}} = 1.5$ for KS 1731–260. Reducing the surface gravity or increasing the accretion rate allows smaller values of Q_{imp} . Impurity scattering sets the thermal conductivity of the inner crust, and so our measurement of Q_{imp} refers to the conductivity in the inner crust, particularly close to neutron drip where the thermal time corresponds to the time of the break in the cooling curve. Interestingly, the values of Q_{imp} derived for both KS 1731–260 and MXB 1659–29 are very similar, and may indicate that a robust outcome of nuclear processing in an accreted crust is an inner crust impurity parameter of order unity, as suggested by calculations of nuclear transitions in the inner crust (Jones 2005; Gupta et al. 2008).
3. The flux required to match the power-law slope between the first and second observations is much larger, however, than expected from models of deep heating (Gupta et al. 2007; Haensel & Zdunik 2008). For KS 1731–260, we find that the lightcurve at ≥ 100 d post-outburst can be fit using standard models of deep heating, if the accretion rate is larger than our esti-

mate of 10^{17} g s^{-1} , in agreement with the findings of Shternin et al. (2007). We do not find such a solution for MXB 1659–29, however; indeed setting the outer boundary condition to $T_b = T_b(T_{\text{eff}})$ drives the outburst accretion rate to roughly the Eddington limit. To obtain an adequate fit to the data, we require the temperature in the outer crust to be decreasing inwards, implying that an inward-directed heat flux enters the crust from the top. Moreover, our Markov Chain Monte Carlo fits with our simplified model (§ 3) find best fit solutions with rather large values of T_b , so that the temperature profile is inverted. Our interpretation therefore differs slightly from that of Shternin et al. (2007). This interpretation depends, however, on the first data points in each cooling curve, and so could be relaxed if these data points are contaminated, by residual accretion for example. Our calculations show that observations taken within the first two weeks following extended outbursts are ideal for mapping out the nuclear heating in the outer crust. It is this shallow heating that is most critical for determining the ignition depth of superbursts (Gupta et al. 2007). We shall investigate the heating required to maintain the inferred high T_b , along with its implications for nuclear processes in the neutron star ocean, in a follow-up paper.

We thank Chuck Horowitz, Ed Cackett, Nathalie Degenaar, Sanjay Reddy, Andrew Steiner, Lars Bildsten, Gil Holder, Bob Rutledge, and Sanjib Gupta for helpful discussions. EFB and AC acknowledge the hospitality of the Institute for Nuclear Theory, where this work took shape, and by the support of the Joint Institute for Nuclear Astrophysics (JINA) under NSF-PFC grant PHY 02-16783. EFB is supported by the National Aeronautics and Space Administration through Chandra Award Number TM7-8003X issued by the Chandra X-ray Observatory Center, which is operated by the Smithsonian Astrophysical Observatory for and on behalf of the National Aeronautics Space Administration under contract NAS8-03060, by NASA award NNX06AH79G, and by NASA ATFP grant NNX08AG76G. AC acknowledges support from an NSERC Discovery Grant, FQRNT, and the Canadian Institute for Advanced Research (CIFAR), and as an Alfred P. Sloan Research Fellow.

REFERENCES

- Aguilera, D. N., Cirigliano, V., Pons, J. A., Reddy, S., & Sharma, R. 2008, ArXiv e-prints
- Ainsworth, T. L., Wambach, J., & Pines, D. 1989, Phys. Lett. B, 222, 173
- Akmal, A., Pandharipande, V. R., & Ravenhall, D. G. 1998, Phys. Rev. C, 58, 1804
- Altamirano, D., Wijnands, R., Degenaar, N., Casella, P., Homan, J., Belloni, T., & Campana, S. 2007, The Astronomer’s Telegram, 1178, 1
- Ayasli, S., & Joss, P. C. 1982, ApJ, 256, 637
- Bassa, C., Jonker, P. G., Nelemans, G., Steeghs, D., Torres, M. A. P., Kuiper, L., in’t Zand, J. J. M., Rea, N., Maccarone, T., Kuulkers, E., Grindlay, J., Wijnands, R., & Mendez, M. 2008, The Astronomer’s Telegram, 1575, 1
- Brown, E. F. 2000, ApJ, 531, 988
- Brown, E. F., Bildsten, L., & Chang, P. 2002, ApJ, 574, 920
- Cackett, E. M., Wijnands, R., Linares, M., Miller, J. M., Homan, J., & Lewin, W. H. G. 2006, MNRAS, 372, 479
- Cackett, E. M., Wijnands, R., Miller, J. M., Brown, E. F., & Degenaar, N. 2008, ApJ, 687, L87
- Caillol, J. M. 1999, J. Chem. Phys., 111, 6538
- Chabrier, G. 1993, ApJ, 414, 695
- Chabrier, G. 1999, in 11th European Workshop on White Dwarfs, ed. J.-E. Solheim & E. G. Meißtas (San Francisco: Ast. Soc. Pacific), 369
- Chabrier, G., & Potekhin, A. Y. 1998, Phys. Rev. E, 58, 4941
- Degenaar, N., Wijnands, R., Wolff, M. T., Ray, P. S., Wood, K. S., Homan, J., Lewin, W. H. G., Jonker, P. G., Cackett, E. M., Miller, J. M., & Brown, E. F. 2009, MNRAS, in press
- Dewitt, H., & Slattey, W. 1999, Contributions to Plasma Physics, 39, 97
- Farouki, R., & Hamaguchi, S. 1993, Phys. Rev. E, 47, 4330
- Galloway, D. K., Muno, M. P., Hartman, J. M., Psaltis, D., & Chakrabarty, D. 2008, ApJS, 179, 360
- Gnedin, O. Y., Yakovlev, D. G., & Potekhin, A. Y. 2001, MNRAS, 324, 725
- Gregory, P. C. 2005, ApJ, 631, 1198
- Gudmundsson, E. H., Pethick, C. J., & Epstein, R. I. 1983, ApJ, 272, 286
- Gupta, S., Brown, E. F., Schatz, H., Möller, P., & Kratz, K. 2007, ApJ, 662, 1188
- Gupta, S. S., Kawano, T., & Möller, P. 2008, Physical Review Letters, 101, 231101
- Haensel, P., & Zdunik, J. L. 1990, A&A, 227, 431
- . 2003, A&A, 404, L33

- , 2008, *A&A*, 480, 459
- Hansen, B. 2004, *Phys. Rep.*, 399, 1
- Heney, L., & L'Ecuyer, J. L. 1969, *ApJ*, 156, 549
- Homan, J., van der Klis, M., Wijnands, R., Belloni, T., Fender, R., Klein-Wolt, M., Casella, P., Méndez, M., Gallo, E., Lewin, W. H. G., & Gehrels, N. 2007, *ApJ*, 656, 420
- Horowitz, C. J., Berry, D. K., & Brown, E. F. 2007, *Phys. Rev. E*, 75, 066101
- Horowitz, C. J., Caballero, O. L., & Berry, D. K. 2008a, *Phys. Rev. E*, in press
- Horowitz, C. J., Dussan, H., & Berry, D. K. 2008b, *Phys. Rev. C*, 77, 045807
- in 't Zand, J., Heise, J., Smith, M. J. S., Cocchi, M., Natalucci, L., & Celidonio, G. 1999, *IAU Circ.*, 7138, 1
- Itoh, N., & Kohyama, Y. 1993, *ApJ*, 404, 268
- Jones, P. B. 2005, *Phys. Rev. D*, 72, 083006
- Jonker, P. G., Bassa, C. G., Nelemans, G., Juett, A. M., Brown, E. F., & Chakrabarty, D. 2006, *MNRAS*, 368, 1803
- Lattimer, J. M., van Riper, K. A., Prakash, M., & Prakash, M. 1994, *ApJ*, 425, 802
- Leinson, L. B., & Perez, A. 2006, *Phys. Lett. B*, 638, 114
- Levenfish, K. P., & Yakovlev, D. G. 1994, *Astonomy Reports*, 38, 247
- Lewin, W. H. G., Hoffman, J. A., Doty, J., & Liller, W. 1976, *IAU Circ.*, 2994, 2
- Oyamatsu, K., & Iida, K. 2007, *Phys. Rev. C*, 75, 015801
- Piro, A. L., Arras, P., & Bildsten, L. 2005, *ApJ*, 628, 401
- Potekhin, A. Y., Baiko, D. A., Haensel, P., & Yakovlev, D. G. 1999, *A&A*, 346, 345
- Potekhin, A. Y., & Chabrier, G. 2000, *Phys. Rev. E*, 62, 8554
- Potekhin, A. Y., Chabrier, G., & Yakovlev, D. G. 1997, *A&A*, 323, 415
- Press, W. H., Teukolsky, S. A., Vetterling, W. T., & Flannery, B. P. 1992, *Numerical Recipes in FORTRAN* (Cambridge: Cambridge University Press)
- Rutledge, R. E., Bildsten, L., Brown, E. F., Pavlov, G. G., Zavlin, V. E., & Ushomirsky, G. 2002, *ApJ*, 580, 413
- Sakano, M., Koyama, K., Murakami, H., Maeda, Y., & Yamauchi, S. 2002, *ApJS*, 138, 19
- Schatz, H., Bildsten, L., Cumming, A., & Wiescher, M. 1999, *ApJ*, 524, 1014
- Schinder, P. J., Schramm, D. N., Wiita, P. J., Margolis, S. H., & Tubbs, D. L. 1987, *ApJ*, 313, 531
- Sedrakian, A., Mütter, H., & Schuck, P. 2007, *Phys. Rev. C*, 76, 055805
- Shternin, P. S., Yakovlev, D. G., Haensel, P., & Potekhin, A. Y. 2007, *MNRAS*, 382, L43
- Steiner, A. W., & Reddy, S. 2009, *Phys. Rev. C*, 79, 015802
- Sunyaev, R. 1989, *IAU Circ.*, 4839, 1
- Thorne, K. S. 1977, *ApJ*, 212, 825
- Timmes, F. X., & Swesty, F. D. 2000, *ApJS*, 126, 501
- Urpin, V. A., & Yakovlev, D. G. 1980, *Soviet Ast.*, 24, 126
- Ushomirsky, G., & Rutledge, R. E. 2001, *MNRAS*, 325, 1157
- Wijnands, R., Guainazzi, M., van der Klis, M., & Méndez, M. 2002, *ApJ*, 573, L45
- Wijnands, R., Homan, J., Miller, J. M., & Lewin, W. H. G. 2004, *ApJ*, 606, L61
- Wijnands, R., Miller, J. M., Groot, P. J., Markwardt, C., Lewin, W. H. G., & van der Klis, M. 2001, *ApJ*, 560, L159
- Wijnands, R., Nowak, M., Miller, J. M., Homan, J., Wachter, S., & Lewin, W. H. G. 2003, *ApJ*, 594, 952
- Yakovlev, D. G., Kaminker, A. D., Gnedin, O. Y., & Haensel, P. 2001, *Phys. Rep.*, 354, 1

APPENDIX

CRUST MICROPHYSICS

In this Appendix, we describe how we calculate the different pieces of microphysics that go into the crust models.

Equation of state and composition profile

We compute the equation of state for the degenerate, relativistic electrons by interpolation from tables of the free energy (Timmes & Swesty 2000). For the ions we compute the EOS using the free energy fit of Chabrier & Potekhin (1998) for the liquid state and the fit of Farouki & Hamaguchi (1993) for the crystalline state. With this choice of fits, the freezing point occurs where the free energies in the liquid and solid phase are equal, namely $\Gamma \equiv Z^2 e^2 / (akT) = 178$, where a is the ion-sphere radius. Note that our fit to the liquid-phase free energy does not include corrections (Potekhin & Chabrier 2000) based on recent Monte Carlo simulations (Dewitt & Slattery 1999; Caillol 1999). As a result, our liquid-phase free-energy is slightly larger (by 0.005% at $\Gamma = 175$) than the expression of Potekhin & Chabrier (2000), and our freezing point is slightly higher than the value of $\Gamma = 175 \pm 0.4$ determined by Potekhin & Chabrier (2000). Although we use the value of Γ at the freezing point determined by the ion free energy for a one-component plasma (OCP), it is important to note that the freezing point may differ significantly from this value because of polarization of the electron background (Potekhin & Chabrier 2000) and because the crust consists of a mixture of isotopes. Indeed, recent molecular dynamics simulations (Horowitz et al. 2007) find that the freezing temperature for a mixture appropriate for X-ray burst ashes is smaller than the OCP, with $\Gamma \approx 250$ at freezing.

We include the Debye reduction in the ion specific heat using an interpolation formula, and compute the Debye temperature according to Chabrier (1993). In the inner crust, we compute the neutron specific heat as that of a degenerate gas, with suppression due to the pairing interaction (Levenfish & Yakovlev 1994). For the 1S_0 pairing of free neutrons in the inner crust, we approximate the critical temperature as a Gaussian in the neutron Fermi wavevector, which approximates the calculation of Ainsworth et al. (1989). The crust temperatures achieved in the models presented here lie below the critical temperature throughout most of the crust, and the neutrons do not contribute significantly to the total specific heat.

The composition of accreting neutron star crusts has been calculated previously by Haensel & Zdunik (2008) and Gupta et al. (2007). They find that the composition of the crust changes abruptly with depth, at locations corresponding to thresholds for electron capture or pycnonuclear reactions. Rather than model the neutron star crust as a series of distinct layers, we instead fit the composition so that Z and A are smoothly varying functions of p . This approximation has a negligible effect on our results, but makes the integration simpler as it avoids jumps in the thermal properties. In the outer crust, we set the mass number A and compute Z in order to maintain β -equilibrium. Using a simple liquid-drop model for the nuclear binding energy,

$$B(A, Z) = a_V A - a_S A^{2/3} - a_A \frac{(N - Z)^2}{A} - a_C \frac{Z^2}{A^{1/3}}, \quad (\text{A1})$$

and minimizing the nucleon-specific Gibbs free energy $G = Y_e \mu_e - B(A, Z)/A$ of a cell containing a nucleus and Z electrons with respect to Z for a fixed A , we obtain the electron fraction Y_e in the outer crust as a function of electron chemical potential μ_e ,

$$Y_e \approx \left(\frac{1}{2} - \frac{\mu_e}{8a_A} \right) \left(1 + \frac{a_C A^{2/3}}{4a_A} \right)^{-1}, \quad (\text{A2})$$

where we take³ $a_A = 23.43$ MeV and $a_C = 0.715$ MeV. This formula accurately reproduces Y_e in the crust models computed by Gupta et al. (2007).

In the inner crust, the relation between chemical potential, Y_e , and the abundance of free neutrons Y_N becomes more complicated. We find that the tables in Haensel & Zdunik (2008) are adequately fit by defining A_{tot} as the total number of nucleons (including free neutrons) per nucleus and setting $Z/A_{\text{tot}} \propto p^{-2/3}$ and A_{tot} increasing as $A_{\text{tot}} \propto p^{2/3}$ up to a maximum value set by the total number of pycnonuclear reactions that occur in the crust. We set a floor to Z/A_{tot} of 0.03, and take $A = \max(A_{\text{outer}}, 0.15A_{\text{tot}})$, where A_{outer} is the mean mass number in the outer crust. Figure 15 shows an example of a crust composition with $A_{\text{outer}} = 56$ and $A_{\text{tot,max}} = 896$ in the inner crust, where we choose $A_{\text{tot,max}}$ to agree with the calculation of Haensel & Zdunik (2008, Fig. 15, *open circles*).

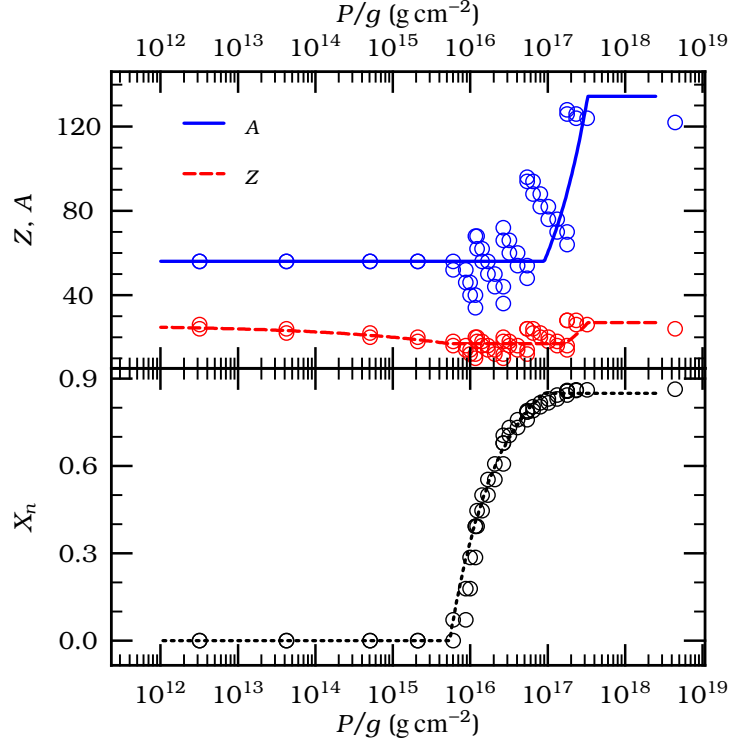


FIG. 15.— Model of composition in the crust: nuclear charge (*top panel, dashed line*) and mass (*top panel, solid line*), and mass fraction of free neutrons (*bottom panel*), as functions of depth coordinate P/g . The composition from Haensel & Zdunik (2008) is shown (*open circles*) for comparison.

Nuclear heating and neutrino cooling

Following Brown (2000), we define a smooth heating distribution in the crust, rather than resolving the heating from individual reaction layers. We choose our heating function to be such that $dL_{\text{nuc}}/d \ln y = \text{const}$, and we do this separately in both the inner crust, and in the outer crust where the pressure is $P > 10^{27}$ ergs cm^{-3} . The integrated nuclear luminosity is plotted in Fig. 16. We normalized the heat distribution so that the total heat deposited, per accreted nucleon, into the inner crust is 1.5 MeV (cf. Haensel & Zdunik 1990, 2003, 2008) and the total heat deposited, per accreted nucleon, into the outer crust is 0.2 MeV (cf. Gupta et al. 2007).

For the neutrino cooling, our model includes (for a review of neutrino emission mechanisms, see Yakovlev et al. 2001) neutrino cooling from electron-nucleus bremsstrahlung. The neutrino emissivity from neutrons paired in the 1S_0 state in the inner crust is suppressed by a factor $(v_F/c)^2$ (Leinson & Perez 2006; Sedrakian et al. 2007). Recent calculations (Steiner & Reddy 2009) show that this suppression follows from conservation of baryon vector current. The pair, photo, and plasmon emissivities (Schinder et al. 1987) do not contribute substantially at the temperatures of interest.

Thermal conductivities

Our implementation of the thermal conductivities mediated by electron-ion scattering follows that of Potekhin et al. (1999) and Gnedin et al. (2001). We compute the electron thermal transport in the relaxation-time approximation,

$$K = \frac{\pi^2 n_e k_B^2 T}{3 m_e^* \nu}, \quad (\text{A3})$$

where $m_e^* = (p_F^2/c^2 + m_e^2)^{1/2}$, with p_F being the Fermi momentum, and ν is the scattering frequency. In the ocean, ν is set by electron-ion scattering. As the ions crystallize, electron-phonon scattering mediates the thermal transport. Where the temperature

³ We obtain values for a_A and a_C by fitting experimental binding energies using the calculator at <http://128.95.95.61/~intuser/1d.html>.

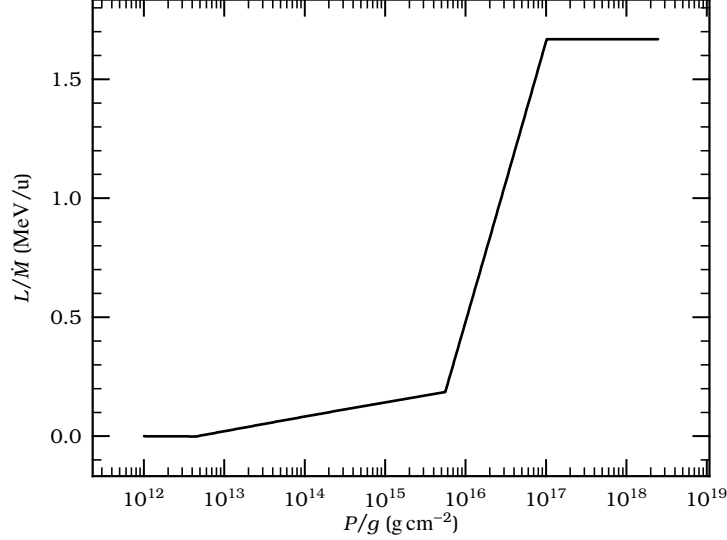


FIG. 16.— Integrated nuclear heating, divided by the proper mass accretion rate, in the crust as a function of column.

is above the Debye temperature, the scattering frequency is approximately

$$\nu_{ep} \approx 13\alpha \frac{k_B T}{\hbar}, \quad (\text{A4})$$

where $\alpha = e^2/(\hbar c)$ is the fine-structure constant. In the inner crust, the electron-ion scattering frequency is strongly reduced for $T < T_p$, the plasma temperature, and impurity scattering becomes dominant with scattering frequency

$$\nu_{eQ} = \frac{4\pi Q_{\text{imp}} e^4 n_{\text{ion}}}{p_F^2 v_F} \Lambda_{\text{imp}}, \quad (\text{A5})$$

where p_F and v_F are the momentum and velocity of electrons at the Fermi surface and the impurity parameter $Q_{\text{imp}} \equiv n_{\text{ion}}^{-1} \sum_i n_i (Z_i - \langle Z \rangle)^2$ measures the distribution of nuclide charge numbers. Although we do include electron-electron scattering (Urpin & Yakovlev 1980; Potekhin et al. 1997) in our calculation, it does not affect the overall thermal conductivity.

For the Coulomb logarithm term Λ_{imp} we use the formula of Potekhin et al. (1999) with the modification that the structure factor is set to unity, reflecting the lack of long-range correlations in the impurities. With this modification Λ_{imp} becomes (Potekhin, private communication)

$$\Lambda_{\text{imp}} = \frac{1}{2} \left\{ \left[1 + 2\beta^2 \frac{q_s^2}{2k_F^2} \right] \ln \left(1 + \frac{4k_F^2}{q_s^2} \right) - \beta^2 - \frac{1 + \beta^2 (q_s/2k_F)^2}{1 + (q_s/2k_F)^2} \right\}, \quad (\text{A6})$$

where $k_F = p_F/\hbar$ is the Fermi wavevector, $\beta = v_F/c$ is the Fermi velocity, and $q_s \approx k_{\text{TF}}$ is the Thomas-Fermi wavevector. As noted by Brown et al. (2002), this gives a result for the Coulomb logarithm that is similar to that proposed by Itoh & Kohyama (1993). The two formulae agree if one makes the substitution $k_F a \rightarrow k_F/(k_{\text{TF}}/2)$, where a is the mean inter-nuclei spacing, in the fit by Itoh & Kohyama (1993). The Thomas-Fermi screening length exceeds the inter-nuclei spacing and produces a larger Λ_{imp} (by about a factor of 2) and hence a lower thermal conductivity than does the fit by Itoh & Kohyama (1993). Molecular dynamics simulations (Horowitz et al. 2008a) using a mixture of rp-process ashes (Gupta et al. 2007), find that the impurities are not distributed uniformly. As a result, Horowitz et al. (2008a) compute a thermal conductivity that is $\approx 30\%$ lower than that computed assuming a one-component plasma and impurities computed with the static structure factor of Itoh & Kohyama (1993).

Finally, Aguilera et al. (2008) recently calculated the thermal conductivity in the inner crust due to superfluid heat conduction. Their Figure 2 shows that, for $T = 10^8$ K, superfluid heat conduction is comparable to heat conduction by electrons for $\rho_{\text{nd}} < \rho \lesssim 2\rho_{\text{nd}}$, where ρ_{nd} is the neutron drip density, and less important at lower temperatures. Therefore, we do not expect that our results would change significantly if superfluid heat conduction was included, unlike the case of magnetars, for which the strong magnetic field suppresses electron transport perpendicular to the magnetic field.